Cell Reports

Decoding distributed oscillatory signals driven by memory and perception in the prefrontal cortex

Graphical abstract

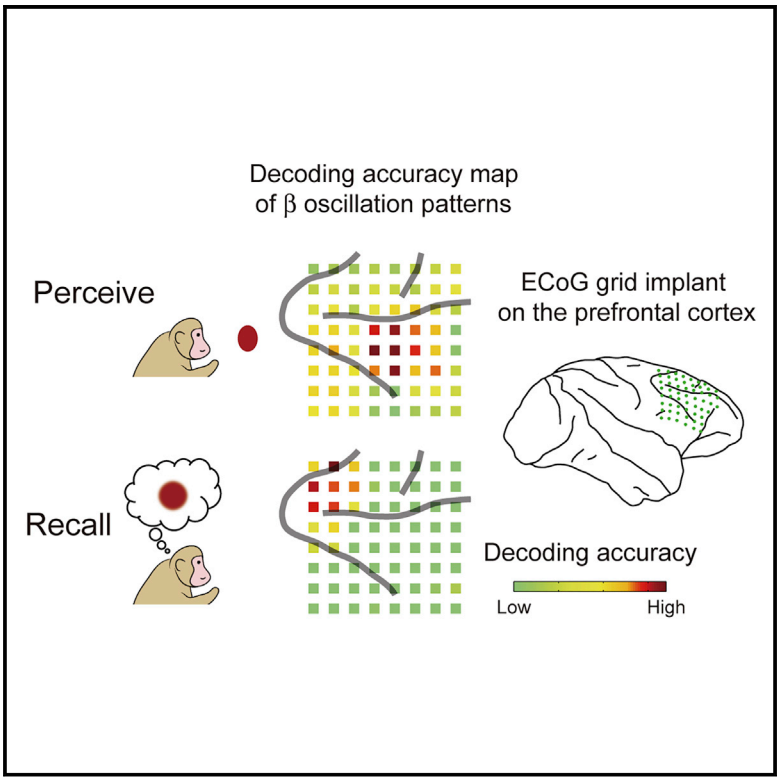

Authors

Hisashi Tanigawa, Kei Majima, Ren Takei, ..., Takafumi Suzuki, Yukiyasu Kamitani, Isao Hasegawa

Correspondence

isaohasegawa@med.niigata-u.ac.jp

In brief

Tanigawa et al. show that dynamically changing neural oscillation patterns of specific frequencies in the macaque prefrontal cortex (PFC) carry mutually distinct information about the same color of memory-recalled target and perceived object. This suggests that the prefrontal oscillations distinguish between perceptual experiences driven by internal memory and external perception.

Highlights

- Frequency-specific oscillatory patterns in the PFC encode the perceived color
- PFC oscillatory patterns also encode the memory-recalled target color
- Oscillatory patterns encoding the recalled color change dynamically over time
- Topographies of oscillatory patterns driven by memory and perception are distinct

Tanigawa et al., 2022, Cell Reports *39*, 110676
April 12, 2022 © 2022 The Authors.
https://doi.org/10.1016/j.celrep.2022.110676

CellPress

Cell Reports

CellPress
OPEN ACCESS

Report

Decoding distributed oscillatory signals driven by memory and perception in the prefrontal cortex

Hisashi Tanigawa,[1,2,3] Kei Majima,[4,5] Ren Takei,[6] Keisuke Kawasaki,[2] Hirohito Sawahata,[2,7] Kiyoshi Nakahara,[3,8] Atsuhiko Iijima,[6] Takafumi Suzuki,[9,10] Yukiyasu Kamitani,[4,5] and Isao Hasegawa[2,3,11,*]

[1]Department of Neurosurgery of the Second Affiliated Hospital and Interdisciplinary Institute of Neuroscience and Technology, School of Brain Science and Brain Medicine, Zhejiang University, Hangzhou 310016, China
[2]Department of Physiology, Niigata University School of Medicine, Niigata, Niigata 951-8501, Japan
[3]Center for Transdisciplinary Research, Niigata University, Niigata, Niigata 951-8501, Japan
[4]Graduate School of Informatics, Kyoto University, Yoshida-honmachi, Sakyo-ku, Kyoto 606-8501, Japan
[5]ATR Computational Neuroscience Laboratories, Keihanna Science City, Kyoto 619-0288, Japan
[6]Department of Bio-cybernetics, Faculty of Engineering, Niigata University, Niigata, Niigata 950-2181, Japan
[7]Department of Industrial Engineering, Mechanical and Control Engineering Course, National Institute of Technology (KOSEN), Ibaraki College, Hitachinaka, Ibaraki 312-8508, Japan
[8]Research Center for Brain Communication, Kochi University of Technology, Kami, Kochi 782-8502, Japan
[9]Center for Information and Neural Networks, National Institute of Information and Communications Technology, Suita, Osaka 565-0871, Japan
[10]Osaka University, Suita, Osaka 565-0871, Japan
[11]Lead contact
*Correspondence: isaohasegawa@med.niigata-u.ac.jp
https://doi.org/10.1016/j.celrep.2022.110676

SUMMARY

Sensory perception and memory recall generate different conscious experiences. Although externally and internally driven neural activities signifying the same perceptual content overlap in the sensory cortex, their distribution in the prefrontal cortex (PFC), an area implicated in both perception and memory, remains elusive. Here, we test whether the local spatial configurations and frequencies of neural oscillations driven by perception and memory recall overlap in the macaque PFC using high-density electrocorticography and multivariate pattern analysis. We find that dynamically changing oscillatory signals distributed across the PFC in the delta-, theta-, alpha-, and beta-band ranges carry significant, but mutually different, information predicting the same feature of memory-recalled internal targets and passively perceived external objects. These findings suggest that the frequency-specific distribution of oscillatory neural signals in the PFC serves cortical signatures responsible for distinguishing between different types of cognition driven by external perception and internal memory.

INTRODUCTION

Our daily conscious experience is based on externally driven sensory inputs and internally generated images, such as mental imagery, memory recall, and dreams. In general, these two types of cognitive experiences are distinct phenomena; however, the underlying neural mechanisms that dissociate them remain unclear (Albright, 2012; Dijkstra et al., 2019). Functional magnetic resonance imaging (fMRI) studies in humans using multivariate pattern analysis (MVPA) have suggested that the patterns of activity for identical visual content are similar during actual perception and mental imagery throughout the ventral visual stream (Albers et al., 2013; Horikawa and Kamitani, 2017; Stokes et al., 2009), with the similarities increasing in the higher visual areas (Lee et al., 2012). The prefrontal cortex (PFC) receives and integrates external inputs and internal information (Miller, 2000). The PFC contains representations of perceived visual information, including color and faces (Haile et al., 2019; Tsao et al., 2008). The PFC also emits a top-down signal that triggers the representation of memory-recalled target information in the inferior temporal cortex, the storehouse of visual long-term memory (Hasegawa et al., 1998; Tomita et al., 1999). However, how the PFC represents internally generated and externally driven perceptual experiences is not well understood.

Mounting evidence suggests that the PFC uses neural oscillations as a mechanism for coordinating neural processes in other brain regions via top-down signals to control various cognitive processes, including perception, attention, working memory, and memory retrieval (Clayton et al., 2015; Helfrich and Knight, 2016; Siegel et al., 2012). Furthermore, neural oscillations at different frequencies are thought to coordinate the bottom-up and top-down flow of information between cortical areas (Bastos et al., 2015; Kerkoerle et al., 2014). Therefore, we hypothesized that the spatial patterns of oscillations with specific frequencies in the PFC would differentially represent

This is an open access article under the CC BY license (http://creativecommons.org/licenses/by/4.0/).

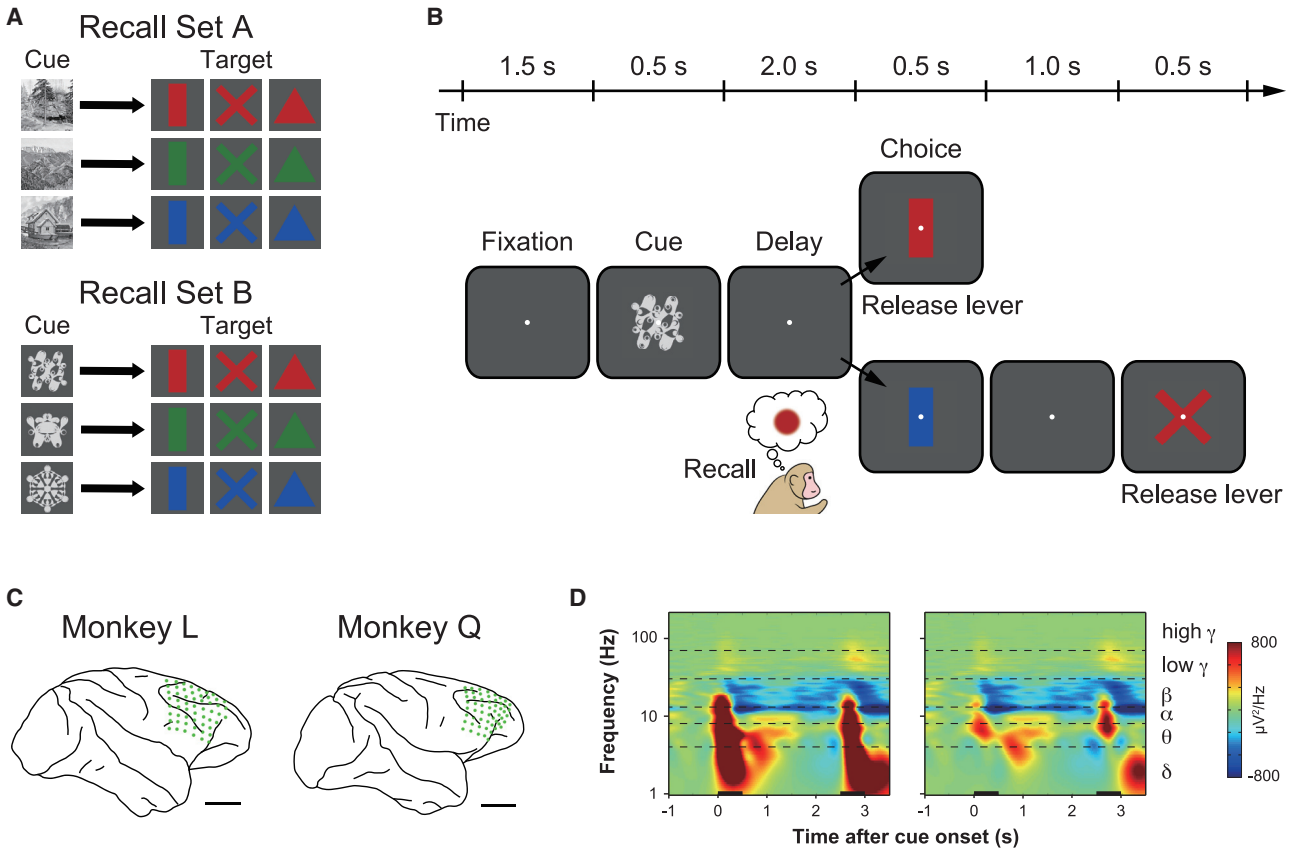

Figure 1. Color-recall task and ECoG recording

(A) Two sets of associations between achromatic stimuli (cue) and colored choice stimuli (target).

(B) Task trial sequence. Following central fixation, a cue stimulus was presented, followed by a delay period and sequence of one to two colored choice stimuli counterbalanced across trials. If the color of the choice stimulus corresponded to the color associated with the prior cue stimulus (target color), as indicated in (A), the monkeys should release the lever to obtain a juice reward.

(C) Lateral views of individual monkey brains showing the position of the ECoG electrode grid, reconstructed by *post mortem* observations. Green dots indicate individual electrodes. Scale bars, 10 mm.

(D) Time-frequency representations of the normalized ECoG powers averaged over all channels in the PFC of monkey L (left) and their induced components, not phase locked to stimulus presentation (right). The thick horizontal black bars at the bottom of each graph represent the cue and choice presentation periods.

the same visual feature of externally and internally derived percept. The current study tested this hypothesis by implanting high-density electrocorticographic (ECoG) electrode arrays in the PFC of macaques to record cortical surface local field potentials during recall and perception tasks and applying MVPA to the oscillatory frequency components of the recorded signals. In addition, because localized regions of stimulus-driven color sensitivity have been reported in the macaque PFC (Haile et al., 2019; Lafer-Sousa and Conway, 2013), we chose color information as the visual content to be decoded by MVPA. Initially, we investigated whether the spatial patterns of oscillations encoded information predicting the color to be chosen that was recalled from long-term associative memory and the color that was passively perceived by external visual stimulation. We then examined the relationship between the distributions of this memory-recalled and externally driven color-related information, as well as their frequency specificity and temporal dynamics.

RESULTS

Behavioral tasks and ECoG from PFC

Two adult macaque monkeys (L and Q) were trained to perform a picture-color association (color-recall) task with two different sets of stimuli (sets A and B, Figure 1A), in which three achromatic cue stimuli specified one of the three isoluminant colors (red, green, and blue) of three different shapes. In each trial of the task (Figure 1B), one of the cue stimuli was presented, and after a delay, the monkeys judged whether the color of the sequentially presented choice stimuli matched the color associated with the cue (target color), regardless of the shape. As controls, the monkeys performed a passive viewing task using the stimuli used as cue or choice stimuli in the color-recall task. While the animals were performing these tasks, we recorded surface local field potentials (LFPs) using a 64-channel ECoG electrode array (2.5 mm interelectrode spacing) implanted subdurally over the monkeys' right lateral PFCs (Figure 1C). Internally

CellPress
OPEN ACCESS

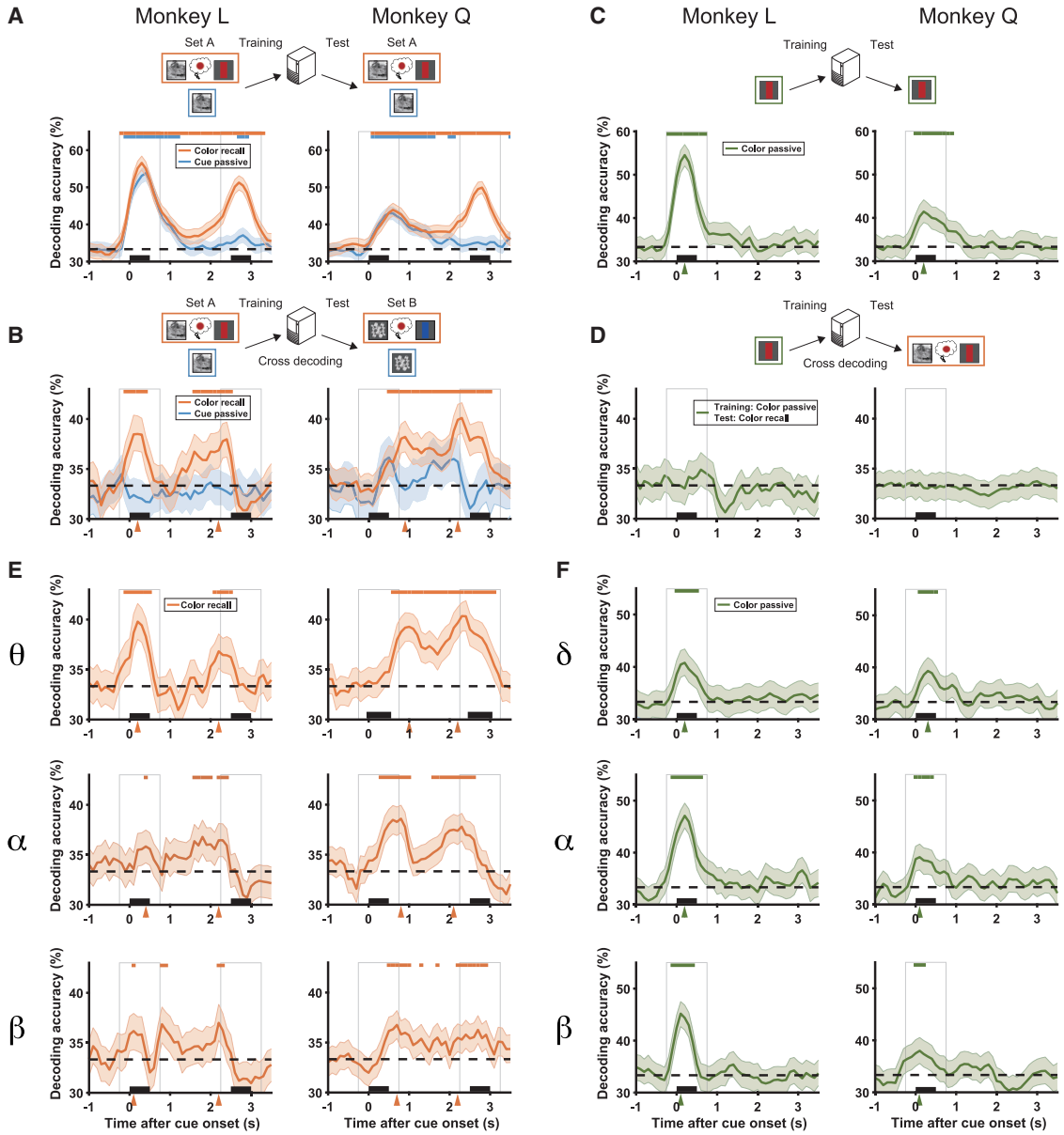

Figure 2. Time courses of decoding recalled color and perceived cue and color

(A) Decoding for cue-associated information in the color-recall task (orange) and passive viewing task (blue) in each monkey using oscillatory powers of the PFC recorded by ECoG. The classifiers were trained and tested on datasets sharing the same stimulus set but different trials. In the orange boxes in the top illustration, examples of a cue stimulus, target color, and first-choice stimulus on a given trial of the color-recall task in the data used to train or test a classifier are shown in order from left to right. For the passive viewing task, only an example of the presented stimulus is shown in the blue or green boxes. The median decoding accuracies obtained from 5,000 iterations were plotted. Shading indicates a 95% confidence interval. The thick horizontal black bars at the bottom of each graph represent the cue and choice presentation periods. However, in the passive viewing task, no choice was presented. The presentation period of the cue and choice stimuli, as well as 250 ms before and after their presentation, are enclosed in gray frames when the analysis window can include those presentation periods. Dotted lines denote the chance level. Colored lines at the top indicate time points at which decoding accuracy was significantly higher than the chance level (bootstrap test; $p < 0.05$; false discovery rate [FDR] correction for 46 time points).

(B) Cross-decoding across different stimulus sets for recalled color (orange) and passively viewed cue stimuli (blue). The orange arrowheads at the bottom indicate the first decoding peak after the cue onset and the last decoding peak in the delay period not influenced by the colored choice stimulus in the color-recall task, respectively.

(C) Decoding of the perceived color in the passive viewing task.

(legend continued on next page)

generated oscillatory components of the LFPs (induced oscillations; Figure 1D), excluding those evoked by the external trial events *per se*, were extracted by subtracting the average signal obtained across the trials from the raw signal recorded in each trial (see STAR Methods; Tallon-Baudry et al., 1999). The spectral powers of induced oscillations in delta, theta, alpha, beta, low-gamma, and high-gamma bands (1–4, 4–8, 8–13, 13–30, 30–70, and 70–200 Hz, respectively) for all channels at each time point were used as input features to train a support vector machine pattern classifier to decode the target color.

Decoding of recalled and perceived color information from PFC oscillatory signals

When a classifier was trained and tested on the dataset from within the same stimulus set (A or B) but across different trials, the decoding performance increased following cue presentation and was significantly above the chance level of 33.3% during most of the delay period, in both animals (Figure 2A, orange). When we analyzed the ECoG signals obtained during the passive viewing of cue stimuli, the performance significantly increased after the cue onset but decreased to the chance level after the offset (Figure 2A, blue), suggesting that the significant decoding observed during the late delay period was specific to the color-recall task. However, it is possible that the increase in decoding performance in the color-recall task reflected information about not only the recalled color but also perceived cue and/or choice stimuli. To eliminate the contribution of these perceived stimuli to the decoding performance, we used cross-decoding analysis (Kriegeskorte, 2011). Trials were divided into four groups according to the cue type (set A or B) and choice type (whether the first-choice stimulus contained the target color or not; Table S1). Then, a classifier was trained on each trial group, and its performance was tested in the other trial group that shared neither cue type nor choice type with the trial group used for training. Using this procedure, whereby the classifier was unable to use information about the perceived cue or choice stimuli, the decoding performance still increased above the level of chance (Figure 2B, orange), suggesting that the spatial patterns of oscillatory activity within the PFC can predict the target color independent of cue type and choice type. Specifically, decoding performance peaked once after the cue onset, then declined, and peaked again during the late phase of the delay period (early and late peaks in Figure 2B, orange arrowheads). The accuracy of cross-decoding across cue sets during passive viewing failed to reach significance (Figure 2B, blue), suggesting that the two cue sets did not evoke shared spatial oscillatory patterns in PFC. We henceforth regard the ability of the classifier to predict the target color before its presentation in cross-decoding as being able to classify the recalled color information, but we address the details of alternative interpretations in the discussion.

We next examined whether recalled and perceived colors induce similar spatial oscillatory patterns in PFC. When both animals passively viewed the colored choice stimuli, the decoding performance for colors using the recorded ECoG signals was higher than the chance level following the stimulus onset (Figure 2C), suggesting that the perceived color was represented in spatial oscillatory patterns of the PFC. We selected the classifier that performed best in predicting perceived colors during the cue period of the passive viewing task (Figure 2C, green arrowheads) and tested whether it could decode the target color in the color-recall task. The decoding performance remained non-significant until the end of the trial (Figure 2D). We also found that classifiers trained at the early and late peaks of decoding in the color-recall task (Figure 2B, orange arrowheads) failed to reach significance in decoding the perceived color throughout the trial of the passive viewing task (Figure S3A). These results suggest that the recall and perception of the same color induced different spatial patterns of oscillatory activity in the PFC.

Frequency and spatial specificities of decoding accuracy

We separately examined the time courses of decoding accuracy in the color-recall task solely based on the power of individual frequency bands as input features to determine which frequency band powers carry information signifying the recalled color. When theta, alpha, or beta powers were used individually, decoding was significant at specific time points in both animals (Figure 2E). In particular, the time course exhibited early and late peaks in theta and alpha bands. Furthermore, the same analysis using the dataset from the passive viewing task using colored stimuli showed that the delta, alpha, and beta patterns showed significant decoding in both animals (Figure 2F). Meanwhile, in each task, decoding accuracy for frequency bands other than those listed above was not significant in both animals or was significant in only one animal (Figures S2A and S2B). Hereafter, we will focus on the results in the frequency bands that were significant in both animals. However, the variability between animals will be discussed in the discussion.

We conducted searchlight analysis (Kriegeskorte et al., 2006) to reveal regional specificity within the PFC for predicting the recalled colors from individual frequency powers at the peak time points. When using theta or alpha powers, we found the regions with the highest decoding accuracy for recalled color information to be anterior to the inferior limb of the arcuate sulcus and ventral to the principal sulcus in both animals at early and/or late peak time points (Figure 3A). According to the sulcus landmarks, these regions were mainly located in the ventrolateral PFC (vlPFC) (Goulas et al., 2017; Petrides and Pandya, 2006), although the time point at which such information appeared varied between animals. In contrast, the beta band consistently exhibited a decoding performance that was highest in the dorsolateral PFC (dlPFC), close to the dorsal tip of the arcuate sulcus in both animals (Figure 3A). For the passive viewing task using colored stimuli, our searchlight decoding revealed peak decoding

(D) Cross-decoding of the recalled color in the color-recall task with the classifier trained to decode the perceived color at the peak time in the top panel (green arrowhead).

(E and F) Decoding of the recalled color (E) and perceived color (F) from the powers of individual frequency bands. Only the time courses in the frequency bands reaching significance in both animals are shown. Those in other frequency bands are shown in Figure S2.

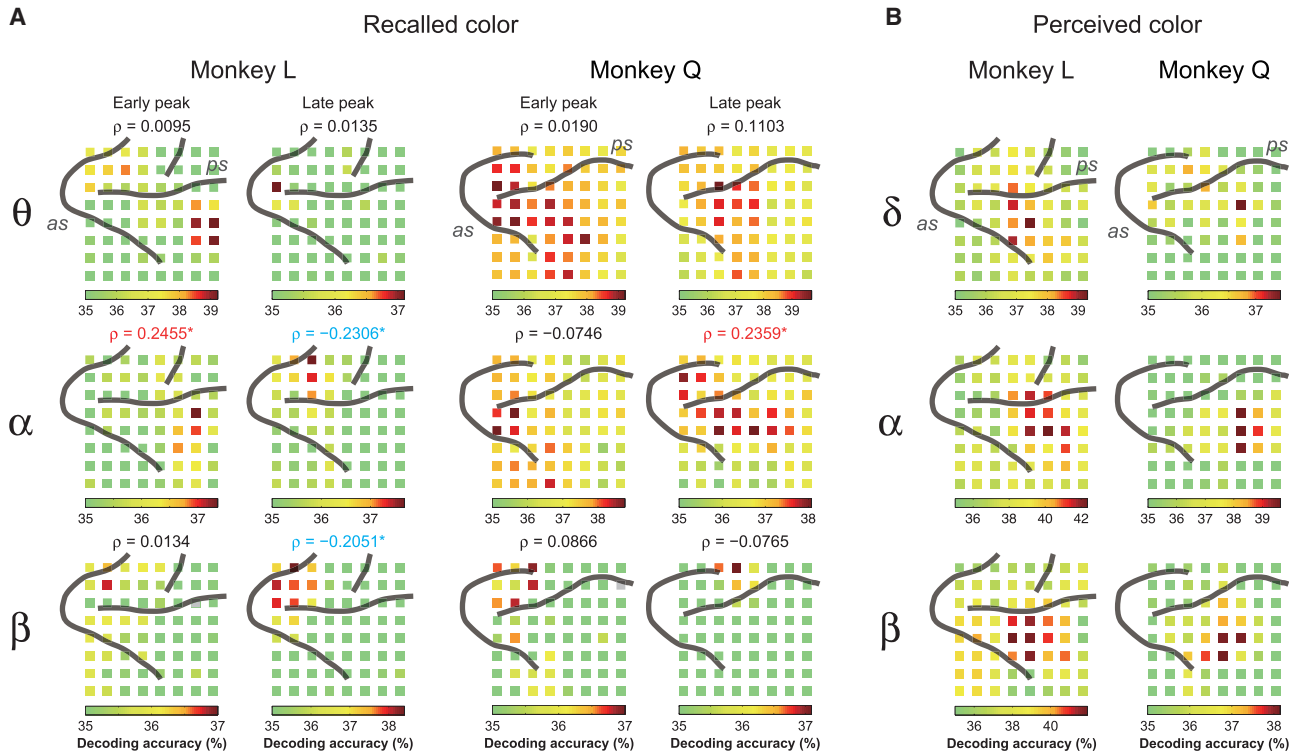

Figure 3. Regions carrying the recalled color and perceived color information in specific frequency bands

Decoding accuracy maps with searchlight classifiers (3 × 3 channels) for recalled (A) and perceived (B) color information based on powers of individual frequency bands in each monkey. Maps are shown at early (left panels) and late (right panels) peak time points in the time courses indicated by arrows in Figures 2E and 2F. Major sulci (*ps*, principal sulcus; *as*, arcuate sulcus) are drawn to compare the positions of the electrode arrays across monkeys. The numbers above the maps for the recalled color in (A) are Spearman's ρ values between those maps and the maps for the perceived color in the same animal and the same frequency band shown in (B) or Figure S2D. Numbers in red and cyan indicate significant positive and negative correlations, respectively (bootstrap test; *$p < 0.05$). Here, we show only the cases of frequency bands that showed significant decoding accuracy at some time point in both animals. Maps for other frequency bands are shown in Figures S2C and S2D. The maximum accuracy adjusted range of the color scale for each map to visualize peaks in the accuracy map for each frequency band. However, to avoid emphasizing low decoding accuracies, if the maximum accuracy was less than 37%, it was adjusted by 37% instead. The maps not adjusted for each map are shown in Figure S4. To avoid double dipping, we only deal with the location of the accuracy peaks, but not the statistics of these maps.

performance in the vlPFC in both animals only when delta, alpha, or beta powers were used (Figure 3B). To investigate whether the distributions of the PFC subregions carrying the recalled and perceived color information were similar or not, we calculated Spearman's rank correlation between their decoding accuracy maps. We found that the maps in delta, theta, and beta bands were not significantly correlated in both animals (Figure 3A; Table S2; $p > 0.05$; two-sided bootstrap test). This finding indicates that the spatial distributions of these two types of color information in the PFC were not similar for these frequency bands. On the other hand, the alpha maps for recalled and perceived color information were significantly correlated in both animals in early or late peak time points (Figure 3A; Table S2; $p < 0.05$; two-sided bootstrap test). Therefore, we examined the time course of cross-decoding using only alpha power between the two tasks. However, the decoding performance was not significant until the end of the trial (Figures S3B and S3C). These results suggest that, although the subregions carrying recalled and perceived color information via alpha oscillations overlapped in the PFC, the local configurations of their oscillatory patterns for individual colors were different.

Cross-temporal decoding for recalled color information

Our searchlight analysis also showed that, depending on the frequency band, the accuracy maps for recalled colors tended to differ between the early and late peak time points (Figure 3A), implying that the maps varied over time. Therefore, to investigate the temporal dynamics of the oscillatory neural representation of recalled color information, we conducted cross-temporal decoding (King and Dehaene, 2014), a method that analyzes the extent to which the decoding of a classifier at a given time point generalizes over time. The results showed intermittent significant decoding performance on the diagonal of the cross-temporal decoding matrix at specific frequency bands, common to both animals (Figures 4 and S2E). This result indicates that, in principle, the spatial patterns of oscillatory activity induced by color recall were not stable over time but changed dynamically in the PFC. However, analysis using delta and theta powers in monkey Q showed significant cross-temporal decoding performance, even for time points away from the diagonal, indicating a relatively long temporal generalization. Finally, we examined the temporal generalization performance of cross-decoding between recalled and

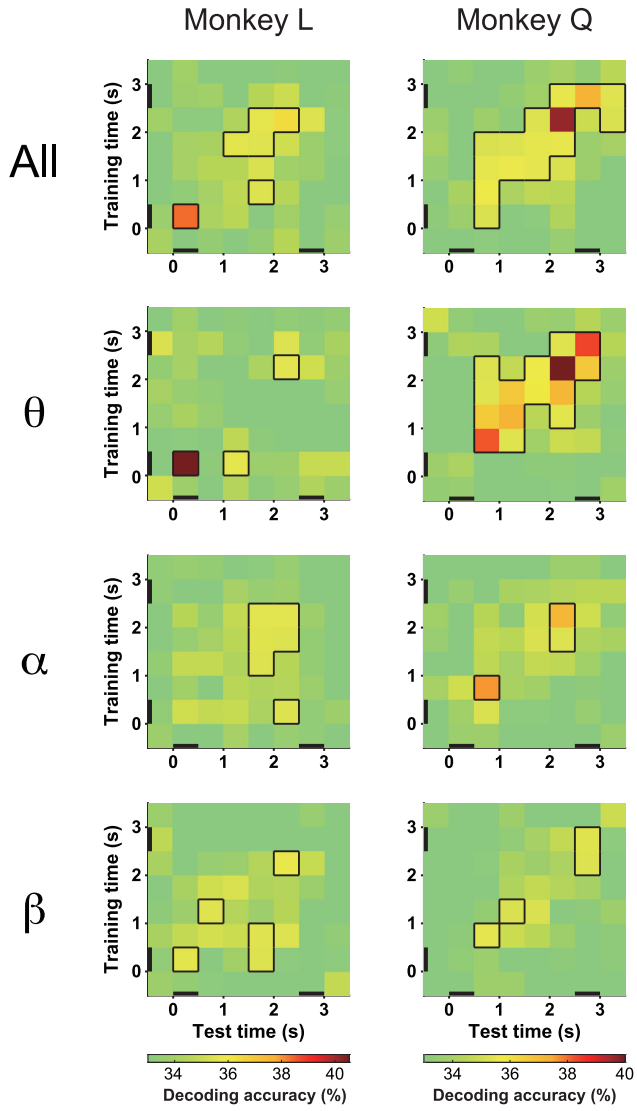

Figure 4. Cross-temporal generalization of recalled color information

Cross-temporal decoding matrix for recalled color information in the color-recall task. A classifier was trained on training data at each 500-ms bin in the color-recall task, and its decoding accuracy was tested at every 500-ms bin of the test data. The y and x axis reflect the classifier training and testing time relative to the cue onset, respectively. Black bars on the axes indicate the cue and choice presentation periods. The color codes indicate the cross-decoding accuracy for recalled color information, and their significance thresholds are shown as contour lines (bootstrap test; $p < 0.05$; FDR correction for 64 time point pairs). Powers of all frequency bands were used as features in the top row, and those of individual frequency bands were used in the lower rows. Only the matrices in the frequency bands that showed significant accuracy in both animals are shown. Those in other frequency bands are shown in Figure S2E.

perceived colors but found no significant cross-temporal generalization at any combination of time points (Figures S3D and S3E). This indicates that the recall and perception of the same color did not share the spatial patterns of oscillatory activity at any time point.

DISCUSSION

Our study showed that the spatial pattern of oscillatory activity spanning the PFC predicts the passively perceived color and the to-be-chosen target color recalled from associative memory. The frequency bands encoding recalled and perceived color information partially overlapped but remained distinct. Specifically, recalled color information was encoded as spatial patterns of oscillations in theta, alpha, and beta bands, while perceived color information was encoded as those in delta, alpha, and beta bands. Notably, a searchlight analysis revealed that the distribution of decoded color information was not similar between them, except for alpha. Moreover, the cross-decoding analysis revealed that both types of color information did not share the configuration of spatial oscillatory patterns, even in the alpha band. These results suggest that the topographical organization of the frequency-specific oscillation patterns generated by associative recall and perception of the same color were different in the PFC. In the sensory cortex, shared representation for these two types of visual information has been proposed based on fMRI studies (Albers et al., 2013; Horikawa and Kamitani, 2017; Stokes et al., 2009). Furthermore, a recent human study using cross-decoding in electroencephalogram (EEG) showed that parieto-occipital alpha oscillations are involved in the shared representations between imagery and perception, while theta and beta oscillations failed to generalize between them (Xie et al., 2020). Together with our results, this EEG study indicates that theta and beta oscillations in the PFC and sensory cortex are good candidates for the neural codes that make sensory visual input and internally generated images different perceptual experiences.

Our "color-recall" task did not require the subject to recall the image of a color *per se* but at minimum to assign a tag specifying the target color associated with the cue based on long-term memory. Possibly, the neural code of that target color tag may represent the color image itself. Alternatively, it could represent more abstract information, such as a criterion for classifying the upcoming choices into three discrete categories or the parametric wavelength of a reference color. In any case, such internally generated neural code might be more or less overlapped with the externally driven perceptual color code in the distributed cortical circuits. We initially aimed to determine their spatial overlap, focusing on the neural oscillations in the PFC. However, the lack of cross-decoding across the recall and passive tasks indicated that the PFC's oscillatory code less likely represents the recalled color image itself.

Many possible explanations for what was decoded from the oscillatory patterns prior to target presentation during the color-recall task have been provided. Previous studies have shown that the activity of PFC neurons prospectively codes internally generated signals anticipating targets (Rainer et al., 1999) and plays a role in signifying the perceptual property of the target, the actual representation of which is presumably distributed downstream in ventral visual cortices (Hasegawa et al., 1998; Simons and Spiers, 2003). The PFC also transforms sensory and internal information into voluntary motor actions (Miller and Cohen, 2001). Such transformed information may be organized as action-oriented representations in support of upcoming behavior

(Myers et al., 2017; Nobre and Stokes, 2019). It is also possible that we decoded the cue category sorted by the target colors (Hasegawa and Miyashita, 2002). However, prediction of the target color based on the cue category class, if any, should be context dependent, because even after learning of the color-recall task with two cue sets in monkey L, cross-decoding accuracy failed at chance in the passive viewing condition (Figure 2B, blue). Thus, in addition to prospective coding of the target color, the PFC's oscillatory activity pattern prior to target color presentation can reflect multiple types of information about the target color other than the color itself, such as preparation for action on the target color and top-down control of color representation. Considering the time-varying maps in searchlight analyses and the poor temporal generalization of decoding for recalled colors, we speculate that what is decoded during the color-recall task might have dynamically changed over time across multiple frequency bands from color memory recall to motor preparation for the anticipated color.

We did not address the results that differed between the two macaques in the study. A possible reason for the variations in results could be that the timing of recall and preparation for action in the color-recall task may have differed across animals. Also, since the data of the passive viewing task with color stimuli were recorded after the training of the color-recall task in monkey L but before the training in monkey Q, the variation in the results could be due to the possibility that the oscillatory activity patterns were reorganized after the training of the color-recall task in one monkey. Such learning effects were indicated by the studies showing changes in spiking activity and neural oscillations in the PFC with working memory task training (Brincat and Miller, 2015; Constantinidis and Qi, 2018).

Neural oscillations in specific frequency bands and oscillatory dynamics, such as phase synchrony and cross-frequency coupling, in the PFC are implicated in many cognitive functions, including working memory and memory recall (Helfrich and Knight, 2016; Miller et al., 2018; Siegel et al., 2012). Beta oscillations represent internally generated contents of working memory and memory recall (Brincat and Miller, 2016; Salazar et al., 2012) and regulate gamma bursts that contribute to the readout and maintenance of working memory (Lundqvist et al., 2016, 2018). By contrast, theta oscillations are proposed to prioritize goal-relevant information in working memory (Riddle et al., 2020; Vries et al., 2020) and to control the representation of working memory content via synchronous oscillations with the posterior sensory cortex (Lara and Wallis, 2014; Liebe et al., 2012). In an associative learning task, theta and alpha/beta synchronous oscillation between the hippocampus and PFC carried error- and correct-trial information, respectively (Brincat and Miller, 2015). Our findings that theta-, alpha-, and beta-band signals can predict memory-recalled color targets are not only consistent with these studies but further suggest that these frequency-specific oscillatory signals are organized topographically in the PFC. Several fMRI studies revealed functional organization of stimulus-driven responses to visual attributes, such as face and color, in PFC (Haile et al., 2019; Lafer-Sousa and Conway, 2013; Tsao et al., 2008). We believe that an approach using high-density ECoG with relatively broad cortical coverage has the potential to reveal detailed functional organization of neural-oscillation-mediated, higher order cognitive functions in the PFC.

Limitations of the study

There is a trade-off between the extent of the cortical area covered by a neuronal recording system and its spatial resolution. The area of PFC covered by our multi-channel ECoG grid was 17.5 mm × 17.5 mm^2 centered on the principal sulcus, which was larger than conventional single-unit recordings but smaller than whole-brain imaging methods, such as fMRI, and restricted to the exposed cortical surface. To record neural oscillation patterns from a wider brain region, we need to design a larger and within-sulcal electrode array (Matsuo et al., 2011). It should also be challenged to capture submillimeter profiles of the local neural architecture by designing a higher density ECoG array at the expense of areal coverage in future studies.

STAR★METHODS

Detailed methods are provided in the online version of this paper and include the following:

- KEY RESOURCES TABLE
- RESOURCE AVAILABILITY
  - Lead contact
  - Materials availability
  - Data and code availability
- EXPERIMENTAL MODEL AND SUBJECT DETAILS
  - Animal care and use
- METHOD DETAILS
  - General surgical procedures
- QUANTIFICATION AND STATISTICAL ANALYSIS

SUPPLEMENTAL INFORMATION

Supplemental information can be found online at https://doi.org/10.1016/j.celrep.2022.110676.

ACKNOWLEDGMENTS

We thank Anna W. Roe and Winrich Freiwald for helpful and insightful comments on the manuscript. This work was supported by Strategic Research Program for Brain Sciences from the Ministry of Education, Culture, Sports, Science, and Technology (MEXT) to I.H., Y.K., and T.S.; JSPS KAKENHI grants (23300150, 26242088, and 19H01038 to I.H.; 17H06268 and 17H00891 to K.N.); AMED under grant number JP21wm0525006 to I.H.; and grants from the National Key R&D Program of China (2018YFA0701402), and National Natural Science Foundation of China (31872776), and a Grant-in-Aid for Young Scientists (Start-up) (23800026) from JSPS to H.T.

AUTHOR CONTRIBUTIONS

H.T. and I.H. designed the experiments; H.T. and R.T. performed the experiments; H.S. and T.S. designed and fabricated the electrodes; H.T., K.M., R.T., K.K., K.N., A.I., Y.K., and I.H. analyzed the data; and H.T., K.K., and I.H. wrote the paper.

DECLARATION OF INTERESTS

The authors declare no competing interests.

Received: August 6, 2021
Revised: February 8, 2022
Accepted: March 22, 2022
Published: April 12, 2022

REFERENCES

Albers, A.M., Kok, P., Toni, I., Dijkerman, H.C., and de Lange, F.P. (2013). Shared representations for working memory and mental imagery in early visual cortex. Curr. Biol. *23*, 1427–1431.

Albright, T.D. (2012). On the perception of probable things: neural substrates of associative memory, imagery, and perception. Neuron *74*, 227–245.

Bastos, A.M., Vezoli, J., Bosman, C.A., Schoffelen, J.-M., Oostenveld, R., Dowdall, J.R., De Weerd, P., Kennedy, H., and Fries, P. (2015). Visual areas exert feedforward and feedback influences through distinct frequency channels. Neuron *85*, 390–401.

Benjamini, Y., and Hochberg, Y. (1995). Controlling the false discovery rate: a practical and powerful approach to multiple testing. J. R. Stat. Soc. Ser. B Methodol. *57*, 289–300.

Brincat, S.L., and Miller, E.K. (2015). Frequency-specific hippocampal-prefrontal interactions during associative learning. Nat. Neurosci. *18*, 576–581.

Brincat, S.L., and Miller, E.K. (2016). Prefrontal cortex networks shift from external to internal modes during learning. J. Neurosci. *36*, 9739–9754.

Clayton, M.S., Yeung, N., and Kadosh, R.C. (2015). The roles of cortical oscillations in sustained attention. Trends Cogn. Sci. *19*, 188–195.

Constantinidis, C., and Qi, X.-L. (2018). Representation of spatial and feature information in the monkey dorsal and ventral prefrontal cortex. Front. Integr. Neurosci. *12*, 31.

Dijkstra, N., Bosch, S.E., and Gerven, M.A.J. (2019). Shared neural mechanisms of visual perception and imagery. Trends Cogn. Sci. *23*, 423–434.

Fan, R.-E., Chang, K.-W., Hsieh, C.-J., Wang, X.-R., and Lin, C.-J. (2008). LIBLINEAR: a library for large linear classification. J. Mach. Learn. Res. *9*, 1871–1874.

Fukushima, M., Saunders, R.C., Leopold, D.A., Mishkin, M., and Averbeck, B.B. (2012). Spontaneous high-gamma band activity reflects functional organization of auditory cortex in the awake macaque. Neuron *74*, 899–910.

Goulas, A., Stiers, P., Hutchison, R.M., Everling, S., Petrides, M., and Margulies, D.S. (2017). Intrinsic functional architecture of the macaque dorsal and ventral lateral frontal cortex. J. Neurophysiol. *117*, 1084–1099.

Haile, T.M., Bohon, K.S., Romero, M.C., and Conway, B.R. (2019). Visual stimulus-driven functional organization of macaque prefrontal cortex. Neuroimage *188*, 427–444.

Hasegawa, I., and Miyashita, Y. (2002). Categorizing the world: expert neurons look into key features. Nat. Neurosci. *5*, 90–91.

Hasegawa, I., Fukushima, T., Ihara, T., and Miyashita, Y. (1998). Callosal window between prefrontal cortices: cognitive interaction to retrieve long-term memory. Science *281*, 814–818.

Helfrich, R.F., and Knight, R.T. (2016). Oscillatory dynamics of prefrontal cognitive control. Trends Cogn. Sci. *20*, 916–930.

Horikawa, T., and Kamitani, Y. (2017). Generic decoding of seen and imagined objects using hierarchical visual features. Nat. Commun. *8*, 15037.

Jafarpour, A., Horner, A.J., Fuentemilla, L., Penny, W.D., and Duzel, E. (2013). Decoding oscillatory representations and mechanisms in memory. Neuropsychologia *51*, 772–780.

Jung, T., Makeig, S., Humphries, C., Lee, T., McKeown, M.J., Iragui, V., and Sejnowski, T.J. (2000). Removing electroencephalographic artifacts by blind source separation. Psychophysiology *37*, 163–178.

Kaiju, T., Doi, K., Yokota, M., Watanabe, K., Inoue, M., Ando, H., Takahashi, K., Yoshida, F., Hirata, M., and Suzuki, T. (2017). High spatiotemporal resolution ECoG recording of somatosensory evoked potentials with flexible micro-electrode arrays. Front. Neural Circuits *11*, 20.

Kerkoerle, T.V., Self, M.W., Dagnino, B., Gariel-Mathis, M.-A., Poort, J., van der Togt, C., and Roelfsema, P.R. (2014). Alpha and gamma oscillations characterize feedback and feedforward processing in monkey visual cortex. Proc. Natl. Acad. Sci. U S A *111*, 14332–14341.

King, J.-R., and Dehaene, S. (2014). Characterizing the dynamics of mental representations: the temporal generalization method. Trends Cogn. Sci. *18*, 203–210.

Kriegeskorte, N. (2011). Pattern-information analysis: from stimulus decoding to computational-model testing. Neuroimage *56*, 411–421.

Kriegeskorte, N., Goebel, R., and Bandettini, P. (2006). Information-based functional brain mapping. Proc. Natl. Acad. Sci. U S A *103*, 3863–3868.

Lafer-Sousa, R., and Conway, B.R. (2013). Parallel, multi-stage processing of colors, faces and shapes in macaque inferior temporal cortex. Nat. Neurosci. *16*, 1870–1878.

Lara, A.H., and Wallis, J.D. (2014). Executive control processes underlying multi-item working memory. Nat. Neurosci. *17*, 876–883.

Lee, S.-H., Kravitz, D.J., and Baker, C.I. (2012). Disentangling visual imagery and perception of real-world objects. Neuroimage *59*, 4064–4073.

Liebe, S., Hoerzer, G.M., Logothetis, N.K., and Rainer, G. (2012). Theta coupling between V4 and prefrontal cortex predicts visual short-term memory performance. Nat. Neurosci. *15*, 456–462.

Lundqvist, M., Rose, J., Herman, P., Brincat, S.L., Buschman, T.J., and Miller, E.K. (2016). Gamma and beta bursts underlie working memory. Neuron *90*, 152–164.

Lundqvist, M., Herman, P., Warden, M.R., Brincat, S.L., and Miller, E.K. (2018). Gamma and beta bursts during working memory readout suggest roles in its volitional control. Nat. Commun. *9*, 394.

Matsuda, K., Nagami, T., Sugase, Y., Takemura, A., and Kawano, K. (2017). A widely applicable real-time mono/binocular eye tracking system using a high frame-rate digital camera. In Human-Computer Interaction. User Interface Design, Development and Multimodality. HCI 2017. Lecture Notes in Computer Science, M. Kurosu, ed. (Springer, Cham), pp. 593–608.

Matsuo, T., Kawasaki, K., Osada, T., Sawahata, H., Suzuki, T., Shibata, M., Miyakawa, N., Nakahara, K., Iijima, A., Sato, N., et al. (2011). Intrasulcal electrocorticography in macaque monkeys with minimally invasive neurosurgical protocols. Front. Syst. Neurosci. *5*, 34.

Miller, E.K. (2000). The prefrontal cortex and cognitive control. Nat. Rev. Neurosci. *1*, 59–65.

Miller, E.K., and Cohen, J.D. (2001). An integrative theory of prefrontal cortex function. Annu. Rev. Neurosci. *24*, 167–202.

Miller, E.K., Lundqvist, M., and Bastos, A.M. (2018). Working memory 2.0. Neuron *100*, 463–475.

Myers, N.E., Stokes, M.G., and Nobre, A.C. (2017). Prioritizing information during working memory: beyond sustained internal attention. Trends Cogn. Sci. *21*, 449–461.

Nakahara, K., Adachi, K., Kawasaki, K., Matsuo, T., Sawahata, H., Majima, K., Takeda, M., Sugiyama, S., Nakata, R., Iijima, A., et al. (2016). Associative-memory representations emerge as shared spatial patterns of theta activity spanning the primate temporal cortex. Nat. Commun. *7*, 11827.

Nobre, A.C., and Stokes, M.G. (2019). Premembering experience: a hierarchy of time-scales for proactive attention. Neuron *104*, 132–146.

Oostenveld, R., Fries, P., Maris, E., and Schoffelen, J.-M. (2011). FieldTrip: open source software for advanced analysis of MEG, EEG, and invasive electrophysiological data. Comput. Intell. Neurosci. *2011*, 156869.

Petrides, M., and Pandya, D.N. (2006). Efferent association pathways originating in the caudal prefrontal cortex in the macaque monkey. J. Comp. Neurol. *498*, 227–251.

Rainer, G., Rao, S.C., and Miller, E.K. (1999). Prospective coding for objects in primate prefrontal cortex. J. Neurosci. *19*, 5493–5505.

Riddle, J., Scimeca, J.M., Cellier, D., Dhanani, S., and D'Esposito, M. (2020). Causal evidence for a role of theta and alpha oscillations in the control of working memory. Curr. Biol. *30*, 1748–1754.

Salazar, R.F., Dotson, N.M., Bressler, S.L., and Gray, C.M. (2012). Content-specific fronto-parietal synchronization during visual working memory. Science *338*, 1097–1100.

Siegel, M., Warden, M.R., and Miller, E.K. (2009). Phase-dependent neuronal coding of objects in short-term memory. Proc. Natl. Acad. Sci. U S A *106*, 21341–21346.

Siegel, M., Donner, T.H., and Engel, A.K. (2012). Spectral fingerprints of large-scale neuronal interactions. Nat. Rev. Neurosci. *13*, 121–134.

Simons, J.S., and Spiers, H.J. (2003). Prefrontal and medial temporal lobe interactions in long-term memory. Nat. Rev. Neurosci. *4*, 637–648.

Stokes, M., Thompson, R., Cusack, R., and Duncan, J. (2009). Top-down activation of shape-specific population codes in visual cortex during mental imagery. J. Neurosci. *29*, 1565–1572.

Tallon-Baudry, C., Bertrand, O., Tallon-Baudry, C., and Bertrand, O. (1999). Oscillatory gamma activity in humans and its role in object representation. Trends Cogn. Sci. *3*, 151–162.

Toda, H., Suzuki, T., Sawahata, H., Majima, K., Kamitani, Y., and Hasegawa, I. (2011). Simultaneous recording of ECoG and intracortical neuronal activity using a flexible multichannel electrode-mesh in visual cortex. Neuroimage *54*, 203–212.

Tomita, H., Ohbayashi, M., Nakahara, K., Hasegawa, I., and Miyashita, Y. (1999). Top-down signal from prefrontal cortex in executive control of memory retrieval. Nature *401*, 699–703.

Torrence, C., and Compo, G.P. (1998). A practical guide to wavelet analysis. Bull. Am. Meteorol. Soc. *79*, 61–78.

Tsao, D.Y., Schweers, N., Moeller, S., and Freiwald, W.A. (2008). Patches of face-selective cortex in the macaque frontal lobe. Nat. Neurosci. *11*, 877–879.

Vries, I.E.J., Slagter, H.A., and Olivers, C.N.L. (2020). Oscillatory control over representational states in working memory. Trends Cogn. Sci. *24*, 150–162.

Whittingstall, K., and Logothetis, N.K. (2009). Frequency-band coupling in surface EEG reflects spiking activity in monkey visual cortex. Neuron *64*, 281–289.

Xie, S., Kaiser, D., and Cichy, R.M. (2020). Visual imagery and perception share neural representations in the alpha frequency band. Curr. Biol. *30*, 2621–2627.

STAR★METHODS

KEY RESOURCES TABLE

REAGENT or RESOURCE	SOURCE	IDENTIFIER
Deposited data		
Time-series data of frequency band power	Tanigawa Lab, Hasegawa Lab	Zenodo: https://doi.org/10.5281/zenodo.5970811
Experimental models: Organisms/strains		
Japanese macaque (*Macaca fuscata*)	NBRP "Japanese Monkeys" through the National BioResource Project of the MEXT, Japan.	https://nihonzaru.jp/aboutus_2_e.html
Software and algorithms		
MATLAB R2019a	MathWorks	RRID: SCR_001622
LabView 2009 SP1	National Instruments	RRID: SCR_014325
FieldTrip toolbox (fieldtrip-20190404)	Open Source	RRID: SCR_004849
LIBLINEAR Version 2.21	Open Source	https://www.csie.ntu.edu.tw/~cjlin/liblinear/
iRecHS2 Version 0.360	Open Source	https://staff.aist.go.jp/k.matsuda/eye/
Custom MATLAB code	Tanigawa Lab, Hasegawa Lab	Zenodo: https://doi.org/10.5281/zenodo.5970811

RESOURCE AVAILABILITY

Lead contact

Further information and requests for resources and reagents should be directed to and will be fulfilled by the lead contact, Isao Hasegawa (isaohasegawa@med.niigata-u.ac.jp).

Materials availability

This study did not generate new unique reagents.

Data and code availability

- Processed ECoG data used for the analyses have been deposited at Zenodo and are publicly available. The DOI is listed in the key resources table.
- All original code has been deposited at Zenodo and is publicly available. The DOI is listed in the key resources table.
- Any additional information required to reanalyze the data reported in this paper is available from the lead contact upon request.

EXPERIMENTAL MODEL AND SUBJECT DETAILS

Animal care and use

Two Japanese monkeys (*Macaca fuscata*, age 4–7 years, weight 5.6-7.1 kg, one female, monkey L, and one male, monkey Q), provided by NBRP "Japanese Monkeys" through the National BioResource Project of the MEXT, Japan, were used in the study. All monkeys were housed in standard primate cages in an air-conditioned room under a 14:10-h light-dark cycle with environmental enrichment that allowed them to live comfortably. The monkeys were given primate food supplemented with fruits and vegetables. The experimental protocol was approved by the Institutional Animal Care and Use Committee of Niigata University (Permission number 27-184-1). All animal procedures conformed to the Act on Welfare and Management of Animals in Japan, Fundamental Guidelines for Proper Conduct of Animal Experiment and Related Activities in Academic Research Institutions under the jurisdiction of the MEXT, Japan, and the National Institute of Health Guide for the Care and Use of Laboratory Animals.

METHOD DETAILS

General surgical procedures

Aseptic surgeries were performed to implant the headpost before behavioral task training requiring head fixation and to implant the ECoG grid before ECoG recording, as described in the following. After premedication with ketamine (50 mg/kg) and medetomidine

(0.03 mg/kg), each animal was intubated with an endotracheal tube and connected to an artificial respirator (A.D.S.1000, Engler Engineering Corp., FL). The venous line was secured using lactated Ringer's solution, and ceftriaxone (100 mg/kg) was dripped as a prophylactic antibiotic. Body temperature was maintained at 37°C using an electric heating mat. A vacuum fixing bed (Vacuform, B.u.W.Schmidt GmbH, Garbsen, Germany) was used to maintain the position of the body. Oxygen saturation, heart rate, and end-tidal CO_2 were continuously monitored (Surgi Vet, Smiths Medical PM Inc., London, UK) throughout surgery to adjust the levels of anesthesia. The skull was fixed with a stereotactic frame (Narishige, Tokyo, Japan) for the headpost implant or a three-point fastening device (Integra Co., NJ) with a custom-downsized attachment for macaques for the ECoG grid implant. The skin and muscles over the target location were removed after local lidocaine injection. For the headpost implant, a titanium headpost (Gray Matter Research, MT) was attached to the skull and secured with resin and bone screws. For the ECoG grid implant, craniotomy and durotomy were performed using a microscope (Ophthalmo-Stativ S22, Carl Zeiss Inc., Oberkochen, Germany) with a CMOS color camera (TS-CA-130MIII, MeCan Imaging Inc., Saitama, Japan). After the implant, the grid was covered by the dura mater, bone flap, and skin, the exposed skull was covered with resin, and the surgery was finished. Postoperatively, the monkeys received ketoprofen as an analgesic for three days, and antibiotics were continued for one week after surgery. The procedures for surgery, anesthesia, and postoperative treatment have already been described previously (Matsuo et al., 2011).

Behavioral tasks. We trained the monkeys to perform a color-recall task (Figure 1B). Each trial began when the monkey held down a lever after an auditory "go" tone was sounded. A fixation point (0.1 ° × 0.1 ° in visual angle, square) appeared at the center of the monitor, and the animal was required to maintain its gaze within ±1.5° of the fixation point until the trial finished; breaks in fixation resulted in the trial being terminated without reward. Following a blank pre-stimulus period (1.5 s), an achromatic cue stimulus was presented (0.5 s); this, in turn, was followed by a blank delay period (2.0 s) and a pseudorandom sequence of one to two colored choice stimulus presentations (0.5 s each) with an interval (1.0 s). To be rewarded with a drop of juice, the animal had to release the lever during a response period (within 1 s after the choice onset) upon being presented with a choice stimulus with the correct color associated with the presented cue (target color). The first choice stimulus had the target color in a random half of trials, and the second choice stimulus had the target color in the remaining half of trials. Apart from this rule, we presented choice stimuli in a pseudorandom order concerning color and shape. An inter-trial interval (2.5 s) was inserted before the next "go" tone. There were two different sets of cue stimuli (Figure 1A): (1) three achromatic scene images (set A; 4.6° wide), and (2) three monochrome Fourier descriptors (set B; ∼3.5° wide). Either type of cue stimuli was used in a recording session. There were nine choice stimuli, with three different shapes in three different colors (Figure 1A; red, green, and blue; ∼3.7° wide). Cue and choice stimuli were presented at the center of the monitor with the fixation point. The colors of choice images, irrespective of image shape, were associated with one of the three cues in each cue type. As a control, the animals also carried out a passive viewing task, in which they had to maintain a fixed gaze on a fixation point during a pre-stimulus period (1.5 s), stimulus presentation (0.5 s), following delay period (2.0 s), and were required to release the lever in order to obtain a juice reward when the fixation point dimmed.

In behavioral analyses, we defined an error as either a lever release following an incorrect choice or failure to release after a correct choice; lever releases before the response period and fixation breaks were regarded as aborted trials, not as error trials. We monitored eye position using an infrared pupil-position monitoring system (iRecHS2 [Matsuda et al., 2017]). Task controls and behavioral data recordings were performed using custom-made software (NS computer service, Japan) running on LabVIEW (National Instruments, TX). For data collection, the animals were required to perform at least 500 successful trials each day and perform the same task for 3 days. The performance on the color-recall task (success rate in non-aborted trials) of monkeys L and Q was 97.2% (set A: 97.9%, set B: 96.5%) and 97.4% (set A: 98.1%, set B: 96.7%). We analyzed only completed trials (see Table S1 for the number of trials used in the analysis). The data of the passive viewing task using colored and cue stimuli were recorded before and after the training of the color-recall task in monkeys Q and L, respectively.

ECoG recording and data processing. To record surface potentials from the PFC, we designed a 64-channel electrode array to cover a 17.5 × 17.5-mm^2 cortical area. We fabricated the electrode array on a 20-μm thick, flexible Parylene-C film using micro-electro-mechanical systems technology, as described previously (Kaiju et al., 2017; Toda et al., 2011). The electrode contacts were gold surfaces of 0.5 × 0.5 mm square exposed from the film. Electrode impedances were typically 20–50 kΩ at 1 kHz. The center-to-center distance between adjacent electrodes was 2.5 mm.

Under sterile surgical conditions, we implanted the electrode array subdurally onto the animals' PFCs, over the lateral prefrontal cortex (Figure 1C). We determined the target location and craniotomy size using preoperative magnetic resonance imaging. A gold reference electrode was placed close to the ECoG array in the subdural space facing the dura. Lead wires from the ECoG array and reference electrodes were connected to micro connectors (Omnetics, MN) in a custom-made titanium chamber fixed to the skull with resin. ECoG signals were amplified and band-pass filtered (Butterworth, 0.7–300 Hz) using a differential amplifier (PBX, Plexon, TX), sampled digitally, and stored on hard-disk drives at a sampling rate 1 kHz.

Data processing was performed using custom MATLAB codes (MathWorks, MA) with the FieldTrip toolbox (https://www.fieldtriptoolbox.org Oostenveld et al., 2011). ECoG signals were segmented, from 4.5 s before to 7.0 s after the onset of the cue stimuli, downsampled to 500 Hz. We eliminated noise components using independent component analysis, implemented in the FieldTrip toolbox (Jung et al., 2000). Signals were re-referenced by subtracting the average values of all electrodes within the same array. We removed signals that were phase-locked to stimulus presentation (i.e., event-related potentials, ERPs) by subtracting the average across trials from each trial to extract internally induced components that were not phase-locked to the stimulus presentation (Figure 1D) (Brincat and Miller, 2015; Siegel et al., 2009; Tallon-Baudry et al., 1999). In Figure 1D, the powers were

normalized by 1/frequency and baseline subtracted (baseline: 0.75–0.25 s before stimulus onset) to increase readability. However, this normalization was not applied to the powers used in the following analyses to preserve information that might have been present in the baseline period (see below). Signal power spectra were calculated at a 1-Hz resolution between 1 Hz and 200 Hz using complex Morlet wavelets (Torrence and Compo, 1998) on a 500-ms analysis window with 100-ms steps, and the time index was aligned to the center of the window. Spectral powers were averaged over each of the following conventionally defined frequency ranges: delta (1–4 Hz), theta (4–8 Hz), alpha (8–13 Hz), beta (13–30 Hz), low gamma (30–70 Hz), and high gamma (70–200 Hz) bands (Fukushima et al., 2012; Nakahara et al., 2016; Whittingstall and Logothetis, 2009).

Once all the recording experiments were completed, the animals were administered an overdose of sodium pentobarbital and transcardially perfused with 4% paraformaldehyde in 0.1 M phosphate buffer (pH 7.4). Electrode locations in the animals' brains were determined postmortem. As ECoG electrode grids were encapsulated in the dura, we photographed the brains before and after dura mater removal and referred to the photographs to identify the electrode locations on the brain's surface.

Pattern classification analysis. For classification analysis, the powers of the individual frequency bands recorded at all electrodes at a given time point were used as input features, unless stated otherwise. In this study, we defined the term "pattern" as the channel-wise spatial configuration of the oscillatory powers used as the input features to be classified at a given time point. We first independently z-normalized the values of each feature using the mean and SD calculated with the training dataset to avoid high-feature values dominating the outcome of the classifier. We did not apply the baseline correction of features in classification analysis to study whether possible contamination in the pre-cue period related to either the upcoming stimulus or the previously seen item (Jafarpour et al., 2013). We used a subset of trials (training dataset) to train a linear support vector machine (LIBLINEAR [Fan et al., 2008]) classifier to discriminate task conditions (e.g., which color the monkey was supposed to respond to in the trial) based on patterns of features. We then quantified the classifier's accuracy to predict the conditions present in an independent subset of trials (test dataset). To minimize the bias of the classifier, we sampled the same number of trials for each task condition in the classification analysis. If the number of trials varied in respect of the conditions, we randomly sampled a subset of trials with more trials to ensure that all conditions had the same number of trials.

To study whether the information about the task condition was available in the pattern of features within one type of task, we assessed the decoding accuracy using a 10-fold cross-validation procedure. In doing so, we trained a classifier using all trials, but one of the ten splits of the dataset and then tested its performance on the remaining one. This procedure was repeated ten times, using a different split for testing each time. The splits used for training did not include the split used for testing for each repetition. The classifier's performance for all trials was considered to be the decoding accuracy of the classifier. In studying a particular aspect of the information about task conditions (e.g., recalled color, perceived color), we used two types of datasets sharing just one aspect of information (e.g., cue, choice) about the task condition. We used one dataset to train a classifier and tested the performance on the other dataset and vice versa (cross-decoding).

In the searchlight analysis (Figures 3, S2D, and S2E), we computed the accuracy based on powers at electrodes within a local sphere (radius 3.6 mm, corresponding to 3 × 3 electrodes) centered on each electrode at a given time point and mapped it onto the center of the sphere to create decoding accuracy maps. We repeated this procedure across all electrodes. In the time course of the decoding accuracy for the recall color in each frequency band (Figures 2B and S2A), we defined the first significant peak after the cue stimulus onset and the latest significant peak earlier than 250 ms before the choice stimulus onset as the early and late peaks and created accuracy maps at those time points (Figures 3A and S2C). We also created accuracy maps for the perceived color (Figures 3B and S2D) at the time point of the first significant peak after the colored stimulus onset in the decoding accuracy time course (Figures 2C and S2A). For frequency bands that did not have significant peaks in the time course as described above, accuracy maps were created at the peak time points in the time course using the powers of all frequency bands (Figures 2B and 2C).

QUANTIFICATION AND STATISTICAL ANALYSIS

All statistical analyses were performed using custom MATLAB codes. We tested the statistical significance of the classifier's performance using the bootstrap method. From the training dataset, we constructed a new dataset by randomly resampling the same number of trials as the dataset with replacement, trained a classifier on that dataset, and tested the classifier's performance on an entire test dataset as described above. This procedure was repeated 5000 times to create a bootstrap distribution of decoding accuracy, and its median and 95% confidence interval were estimated. The proportion of values in that distribution that was smaller than the chance level was calculated as the p value for the null hypothesis that decoding accuracy does not differ from the chance level. If the observed p value was lower than the lowest possible p value achievable with our bootstrap method ($p = 2 \times 10^{-4}$ for 5000 samples), it was set to $p = 2 \times 10^{-4}$. Unless otherwise specified, corrections for multiple comparisons were performed using Benjamini and Hochberg's false discovery rate method (Benjamini and Hochberg, 1995). For the statistics of Spearman's rank correlation between the decoding accuracy maps for the recalled colors and perceived colors (Figures 3, S2C, and S2D), the correlation coefficients of decoding accuracies of 64 channels were calculated on 5000 pairs of maps obtained by the above procedure, and the resulting correlation coefficient distribution was tested to see if it was significantly different from 0 using a two-sided bootstrap test (Table S2). In this analysis, no correction for multiple comparisons was performed. We set our threshold for significance across all tests at $p < 0.05$. The numbers of trials used for the analyses are shown in Table S1.